

# A Geometric Taxonomy of Hallucinations in LLMs

Javier Marín  
 javier@jmarin.info

January 2026

## Abstract

The term "hallucination" in large language models conflates distinct phenomena with different geometric signatures in embedding space. We propose a taxonomy identifying three types: unfaithfulness (failure to engage with provided context), confabulation (invention of semantically foreign content), and factual error (incorrect claims within correct conceptual frames). We observe a striking asymmetry. On standard benchmarks where hallucinations are LLM-generated, detection is domain-local: AUROC 0.76–0.99 within domains, but 0.50 (chance level) across domains. Discriminative directions are approximately orthogonal between domains (mean cosine similarity -0.07). On human-crafted confabulations — invented institutions, redefined terminology, fabricated mechanisms — a single global direction achieves 0.96 AUROC with 3.8% cross-domain degradation. We interpret this divergence as follows: benchmarks capture generation artifacts (stylistic signatures of prompted fabrication), while human-crafted confabulations capture genuine topical drift. The geometric structure differs because the underlying phenomena differ. Type III errors show 0.478 AUROC — indistinguishable from chance. This reflects a theoretical constraint: embeddings encode distributional co-occurrence, not correspondence to external reality. Statements with identical contextual patterns occupy similar embedding regions regardless of truth value. The contribution is a geometric taxonomy clarifying the scope of embedding-based detection: Types I and II are detectable; Type III requires external verification mechanisms.

## 1 Introduction

Large language models generate text through autoregressive next-token prediction, optimizing for the distributional statistics of training corpora [Brown et al., 2020, Touvron et al., 2023, Achiam et al., 2023]. This objective produces fluent continuations without maintaining explicit correspondence to external reality—a characteristic that manifests as hallucination [Ji et al., 2023, Huang et al., 2023]. The phenomenon poses significant challenges for deployment in high-stakes domains, particularly under regulatory frameworks like the EU AI Act, which mandate appropriate accuracy levels and transparency about system limitations [European Parliament, 2024].

Yet “hallucination” is not one phenomenon. The term has become a catch-all for distinct failure modes: a model that ignores provided documents differs fundamentally from one that invents non-existent entities, which differs again from one that provides incorrect details about real concepts [Maynez et al., 2020, Zhang et al., 2024]. These failures have different causes, different consequences, and—as this paper demonstrates—different geometric signatures in the embedding spaces that underlie modern NLP systems.

We argue that progress on hallucination detection requires first untangling what “hallucination” means. The contribution of this paper is a geometric taxonomy that distinguishes hallucination

types by their behavior on the embedding hypersphere  $S^{d-1}$ , and demonstrates that different types require fundamentally different detection approaches.

Our starting point is the Semantic Grounding Index (SGI), which measures whether a response engages with the provided context by computing ratios of angular distances on the unit hypersphere [Marín, 2025]. SGI achieves strong discrimination (Cohen’s  $d = 0.92\text{--}1.28$ ) for detecting *unfaithfulness*—responses that ignore context in favor of parametric memory. However, SGI requires context embeddings, limiting its applicability to retrieval-augmented generation (RAG) settings.

This paper extends the geometric approach to context-free detection. We introduce the Directional Grounding Index ( $\Gamma$ ), which measures alignment between a query-response displacement and expected grounding directions learned from reference examples. Through systematic experiments, we discover that  $\Gamma$ ’s behavior depends critically on what kind of hallucination it encounters, a finding that motivates our geometric taxonomy.

The taxonomy distinguishes three types based on their geometric signatures. **Type I: Unfaithfulness** occurs when the model ignores provided context; geometrically, the response remains angularly proximate to the question rather than departing toward the context. **Type II: Confabulation** occurs when the model invents semantically foreign content; geometrically, the response displacement points away from the manifold of plausible answers. **Type III: Factual Error** occurs when the model provides incorrect details within the correct conceptual frame; geometrically, the response occupies a plausible region but contains wrong information.

Our experiments reveal that Type I and Type II are geometrically detectable with high accuracy, while Type III poses fundamental challenges for embedding-based methods. This clarifies both the possibilities and the limits of geometric hallucination detection.

The paper proceeds as follows. Section 2 reviews related work on hallucination definitions, detection methods, and geometric approaches. Section 3 develops the theoretical framework, including the embedding hypersphere geometry and our detection indices. Section 4 presents the geometric taxonomy with formal definitions. Section 5 describes our experimental methodology. Section 6 presents results, including the critical finding that different hallucination types exhibit qualitatively different geometric behavior. Section 7 discusses implications for research and deployment. Section 8 acknowledges limitations, and Section 9 concludes.

## 2 Related Work

### 2.1 The Contested Meaning of Hallucination

The term “hallucination” entered NLP discourse from neural machine translation, where it described outputs unrelated to source sentences [Lee et al., 2018, Raunak et al., 2021]. In the era of large language models, the term has expanded to cover a heterogeneous collection of failure modes, leading to what Ji et al. [2023] characterize as definitional chaos.

Academic definitions cluster around two poles. Ji et al. [2023] define hallucination as “generated content that is nonsensical or unfaithful to the provided source content,” emphasizing faithfulness to input. Huang et al. [2023] propose “plausible yet nonfactual content,” shifting the reference point to factuality against world knowledge. Maynez et al. [2020] distinguish *intrinsic* hallucinations (contradicting source) from *extrinsic* hallucinations (unverifiable from source), a framework adopted by subsequent work on summarization [Kryscinski et al., 2020, Fabbri et al., 2022].

The practitioner community reveals deeper disagreements. Karpathy [2023] provocatively argues that “hallucination is all LLMs do—they are dream machines,” suggesting the term is misleading because LLMs never retrieve truth but always generate from learned distributions. Hicks et al. [2024] advocate abandoning “hallucination” entirely in favor of “bullshit” in Frankfurt’s philosophical

sense: speech produced without concern for truth [Frankfurt, 2005]. Marcus [2024] argues the anthropomorphic framing obscures the fundamental unreliability of current architectures.

We take a different approach: rather than debating terminology, we operationalize distinctions through geometry. If different failure modes produce different signatures in embedding space, the taxonomy becomes empirically grounded rather than merely definitional.

## 2.2 Detection Methods

Hallucination detection methods vary by what information they access. Methods requiring model internals achieve strong performance: Azaria and Mitchell [2023] showed that hidden-state trajectories differ systematically between truthful and hallucinated generations (AUROC 0.96 on TruthfulQA). Chen et al. [2024] use eigenvalue spectra of response covariance matrices. Liu et al. [2024] probe intermediate layers for calibrated confidence. These approaches access information the model has but doesn’t surface, which is precisely why they work—but API-based deployments provide no such access.

Methods requiring multiple generations sample the model repeatedly and measure consistency. SelfCheckGPT [Manakul et al., 2023] achieves AUC-PR 0.93 by comparing responses across samples. Semantic entropy [Farquhar et al., 2024, Kuhn et al., 2023] clusters responses by meaning and measures distributional entropy (AUROC 0.79 on various benchmarks). These methods are principled but require 5–20 generations per query, making them impractical for production systems processing thousands of requests.

When source documents are available, detection becomes alignment verification. HHEM [Vectara, 2024] achieves 74–77% balanced accuracy using cross-encoder architectures. AlignScore [Zha et al., 2023] reaches AUC-ROC 0.87 with unified alignment functions. SummaC [Laban et al., 2022] and FactCC [Kryscinski et al., 2020] frame detection as natural language inference. LettuceDetect [Kovács and Recsiki, 2025] fine-tunes encoders specifically for RAG hallucination. These methods are effective but require context.

The gap we address is detection without model internals, without multiple generations, and without source documents—using only the geometric structure of embedding space.

## 2.3 Geometric Approaches

Modern sentence transformers are trained via contrastive objectives that explicitly optimize angular relationships on the unit hypersphere [Reimers and Gurevych, 2019, Gao et al., 2021]. Wang and Isola [2020] analyze contrastive learning through alignment (matching pairs cluster) and uniformity (embeddings spread evenly), showing these properties emerge on  $S^{d-1}$ .

Several works exploit this geometry for uncertainty quantification. Catak et al. [2024] apply convex hull analysis to embedding distributions. Oblovatny, R. et al. [2025] found that hallucinated responses exhibit smaller hidden-state deviations from prompts—an observation consistent with what we term “semantic laziness.”

The Semantic Grounding Index [Marín, 2025] introduced angular ratio measurement for context-based detection, achieving large effect sizes (Cohen’s  $d$  up to 1.28) on HaluEval [Li et al., 2023]. SGI demonstrated that the spherical triangle inequality predicts detection performance: effect sizes increase monotonically with question-context angular separation. This paper extends that geometric framework to context-free settings and discovers that different hallucination types have fundamentally different geometric properties.

## 2.4 Benchmarks and Their Construction

Standard benchmarks operationalize hallucination through different construction methods. TruthfulQA [Lin et al., 2022] contains 817 questions targeting common misconceptions, with human-written false answers reflecting beliefs people actually hold. HaluEval [Li et al., 2023] generates hallucinations by prompting LLMs to fabricate plausible-sounding falsehoods across QA, dialogue, and summarization. FactScore [Min et al., 2023] decomposes long-form generations into atomic facts for fine-grained evaluation. FaithBench [Bao et al., 2025] and RAGTruth [Niu et al., 2024] focus on faithfulness in summarization and retrieval-augmented settings.

A critical observation motivates our experiments: most benchmarks construct hallucinations by prompting models to generate false content. This may introduce generation artifacts—systematic differences in how models write when instructed to fabricate versus when generating normally. If so, detection methods might learn to identify these artifacts rather than hallucination per se. We test this hypothesis by comparing benchmark-style hallucinations to human-crafted confabulations.

## 3 Theoretical Framework

### 3.1 The Embedding Hypersphere

Contrastive learning objectives for sentence embeddings decompose into alignment and uniformity terms on the unit hypersphere [Wang and Isola, 2020]. The InfoNCE loss encourages matched pairs to cluster while spreading unrelated points uniformly, inducing structure on  $S^{d-1}$  where  $L_2$ -normalized embeddings reside.

Let  $\phi : \mathcal{S} \rightarrow \mathbb{R}^d$  denote a sentence embedding model mapping strings to  $d$ -dimensional vectors, and let  $\hat{\phi}(s) = \phi(s)/\|\phi(s)\|$  denote the  $L_2$ -normalized representation. The normalized embeddings lie on the unit hypersphere:

$$S^{d-1} = \{x \in \mathbb{R}^d : \|x\| = 1\} \quad (1)$$

This is a compact Riemannian manifold with constant positive curvature [Mardia and Jupp, 2000]. The natural distance metric is the geodesic (great-circle arc length), equivalent to the angular distance:

$$\theta(a, b) = \arccos(\hat{\phi}(a)^\top \hat{\phi}(b)) \quad (2)$$

This angular distance  $\theta \in [0, \pi]$  satisfies all metric axioms on  $S^{d-1}$ , including the triangle inequality [Bridson and Haefliger, 2013]. We note that while cosine similarity is ubiquitous in applications, it does not satisfy the triangle inequality; angular distance is the proper metric for geometric analysis [You, 2025].

### 3.2 The Semantic Grounding Index

For retrieval-augmented generation instances  $(q, c, r)$  with question  $q$ , retrieved context  $c$ , and generated response  $r$ , the Semantic Grounding Index measures how the response positions itself relative to the question and its context [Marín, 2025]:

**Definition 1** (Semantic Grounding Index).

$$SGI(r; q, c) = \frac{\theta(r, q)}{\theta(r, c)} \quad (3)$$

SGI captures the ratio of angular departures: how far the response has traveled from the question relative to its distance from the context. When  $\text{SGI} > 1$ , the response is angularly farther from the question than from the context—it has “departed” toward the context’s semantic territory. When  $\text{SGI} < 1$ , the response remains closer to the question, showing semantic laziness.

The spherical triangle inequality constrains admissible SGI values. For any  $q, c, r \in S^{d-1}$ :

$$|\theta(q, c) - \theta(r, c)| \leq \theta(r, q) \leq \theta(q, c) + \theta(r, c) \quad (4)$$

Dividing by  $\theta(r, c)$  yields bounds on SGI:

$$\left| \frac{\theta(q, c)}{\theta(r, c)} - 1 \right| \leq \text{SGI} \leq \frac{\theta(q, c)}{\theta(r, c)} + 1 \quad (5)$$

These bounds generate a theoretical prediction: SGI’s discriminative power should increase with  $\theta(q, c)$ . When  $q$  and  $c$  are semantically similar (small  $\theta(q, c)$ ), the triangle inequality constrains SGI values near 1 despite of response quality. When  $\theta(q, c)$  is large, the constraint relaxes, allowing greater separation between grounded and ungrounded responses. This prediction has been confirmed empirically [Marín, 2025].

### 3.3 The Directional Grounding Index

SGI requires context embeddings, limiting its applicability. We now develop a context-free detection method based on displacement direction alignment.

Consider a query  $q$  and response  $r$ . The displacement vector  $\delta(q, r) = \hat{\phi}(r) - \hat{\phi}(q)$  captures how the response relates to the query geometrically. We normalize this displacement:

$$\hat{\delta}(q, r) = \frac{\delta(q, r)}{\|\delta(q, r)\|} \quad (6)$$

Given a reference set  $\mathcal{R} = \{(q_i, r_i)\}_{i=1}^N$  of verified grounded query-response pairs, we can characterize the expected displacement direction for grounded responses. The mean displacement direction is:

$$\mu = \frac{1}{N} \sum_{i=1}^N \hat{\delta}(q_i, r_i), \quad \hat{\mu} = \frac{\mu}{\|\mu\|} \quad (7)$$

**Definition 2** (Directional Grounding Index -  $\Gamma$ ).

$$\Gamma(q, r; \mathcal{R}) = \hat{\delta}(q, r)^\top \hat{\mu} \quad (8)$$

$\Gamma$  ranges from  $-1$  to  $+1$ . High values indicate alignment with expected grounding patterns; low or negative values indicate anomalous displacement. The interpretation is geometric: grounded responses should move in a consistent direction from queries, while hallucinations either fail to move appropriately or move in unrelated directions.

An alternative formulation uses local neighborhood structure. For a test query  $q$ , we can compute a query-specific mean direction from its  $k$  nearest neighbors in the reference set:

$$\mu_q = \frac{1}{k} \sum_{(q_i, r_i) \in \mathcal{N}_k(q)} \hat{\delta}(q_i, r_i) \quad (9)$$

**Definition 3** (Local Directional Grounding Index).

$$\Gamma_{local}(q, r; \mathcal{R}, k) = \hat{\delta}(q, r)^\top \hat{\mu}_q \quad (10)$$

This local formulation allows a domain-adaptive detection, potentially capturing that different semantic regions have different grounding geometries. We test whether local sections improve over a global calibration.

### 3.4 Computational Complexity

Both SGI and  $\Gamma$  are computationally efficient. SGI requires three embeddings and two angular distance calculations:  $O(d)$  after embedding.  $\Gamma$  with global  $\mu$  requires one embedding and one dot product:  $O(d)$  after a one-time  $O(Nd)$  computation of  $\mu$ . Local  $\Gamma$  adds a  $k$ -nearest neighbor lookup, which with approximate nearest neighbor indices (e.g., FAISS) costs  $O(\log N)$  per query after  $O(N \log N)$  index construction. For typical parameters ( $d = 768$ ,  $k = 15$ ,  $N = 10,000$ ), both methods add negligible overhead to embedding computation.

## 4 A Geometric Taxonomy of Hallucination

We propose three hallucination types distinguished by their geometric signatures on  $S^{d-1}$ . The taxonomy is grounded in how responses position themselves relative to queries, contexts (when available), and the manifold of plausible answers.

**Definition 4** (Plausibility Manifold). *For a query  $q$ , the plausibility manifold  $\mathcal{P}_q \subset S^{d-1}$  is the region containing embeddings of semantically appropriate responses—both correct answers and plausible errors that use appropriate vocabulary and address the question’s topic.*

The plausibility manifold is not directly observable but can be approximated through reference sets of grounded responses. Its conceptual role is to distinguish responses that are “in the right neighborhood” (potentially wrong but topically appropriate) from responses that are “elsewhere entirely” (semantically foreign to the question).

**Hypothesis 1** (Type I: Unfaithfulness). *When a model ignores provided context and generates from parametric memory, the response remains angularly proximate to the question rather than departing toward the context. Formally, for unfaithful response  $r_u$  given context  $c$ :*

$$\theta(r_u, q) < \theta(r_g, q) \quad \text{and} \quad \text{SGI}(r_u; q, c) < 1 \quad (11)$$

where  $r_g$  denotes a grounded response. This is semantic laziness: the response fails to make the journey toward the context’s semantic territory.

Type I hallucinations are detectable via SGI when context is available. The detection mechanism relies on measuring whether the response engaged with the provided documents.

**Hypothesis 2** (Type II: Confabulation). *When a model invents entities, mechanisms, or concepts that do not exist, the response displacement points away from the plausibility manifold. Formally, for confabulated response  $r_c$ :*

$$r_c \notin \mathcal{P}_q \quad \text{and} \quad \Gamma(q, r_c) \ll \Gamma(q, r_g) \quad (12)$$

The response introduces semantically foreign content, causing displacement in directions unrelated to how grounded responses typically move.

Type II hallucinations are potentially detectable via  $\Gamma$  without context, because confabulations leave the neighborhood of plausible answers entirely.

**Hypothesis 3** (Type III: Factual Error). *When a model provides incorrect details within the correct conceptual frame, the response occupies a plausible region of embedding space. Formally, for factually erroneous response  $r_e$ :*

$$r_e \in \mathcal{P}_q \quad \text{and} \quad \Gamma(q, r_e) \approx \Gamma(q, r_g) \quad (13)$$

The response is semantically similar to correct answers—it uses appropriate vocabulary and addresses the topic—but contains factual errors.

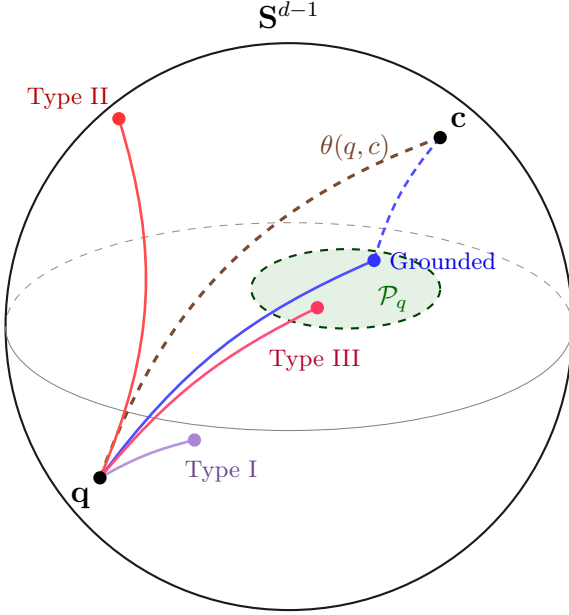


Figure 1: Geometric taxonomy of hallucination types on the embedding hypersphere  $\mathbf{S}^{d-1}$ . Query  $\mathbf{q}$  and context  $\mathbf{c}$  define anchor points. The plausibility manifold  $\mathcal{P}_q$  (green, dashed) contains semantically appropriate responses. A grounded response (blue) departs from  $\mathbf{q}$  toward  $\mathbf{c}$  and lands within  $\mathcal{P}_q$ . Type I unfaithfulness (purple) shows semantic laziness, remaining near  $\mathbf{q}$ . Type II confabulation (red) departs in an unrelated direction, landing outside  $\mathcal{P}_q$ . Type III factual error (orange) reaches  $\mathcal{P}_q$  but occupies a factually incorrect position within the plausible region.

The reason Type III hallucinations resist geometric detection is not an empirical surprise but a theoretical constraint baked into the foundations of distributional semantics since the 1950s. Firth [1957] famously argued that you shall know a word by the company it keeps.” Harris [1954] formalized this behaviour but never claimed that distributional similarity captures truth—only that it captures linguistic co-occurrence structure. These are fundamentally different things. A statement like “FDIC insures deposits up to \$500,000” is factually wrong but semantically indistinguishable from “FDIC insures deposits up to \$250,000”—both occupy similar regions of embedding space as they occur in the same linguistic context. So, our TruthfulQA experimental result (AUROC 0.478) is a prediction confirmed.

Figure 1 illustrates the geometric relationships among Type I, II and III.

## 5 Experimental Methodology

### 5.1 Research Questions

Our experiments address three questions. First, does  $\Gamma$  achieve effective context-free hallucination detection? Second, how does  $\Gamma$ ’s behavior differ across Type I, II and III? Third, does local section estimation improve over global calibration?

### 5.2 Datasets

We use three datasets representing different hallucination construction methods.

**HaluEval QA** [Li et al., 2023] contains 10,000 question-knowledge-answer triples with hallucination labels. Hallucinations are generated by prompting GPT-3.5 to produce plausible-sounding fabrications. We use  $n = 5,000$  samples for primary experiments and the grounded pairs as reference sets for calibrating  $\Gamma$ .

**TruthfulQA** [Lin et al., 2022] contains 817 questions targeting common misconceptions, with human-written truthful and false answers. False answers reflect beliefs people actually hold—imitative falsehoods learned from training data. We use  $n = 800$  paired samples to test whether angular geometry can discriminate factual accuracy when both responses concern the same topic.

**Human-Crafted Confabulations.** We created 142 question-response pairs across three domains: finance (50), medical (50), and legal (42). Each item consists of a factual question, a grounded response obtained from an LLM (Claude Sonnet 4.5), and a human-written confabulation. Confabulations are manually created to represent real-world failure modes where models might confidently state entirely false information.

Confabulation guidelines include: *redefinition* (“P/E ratio stands for Price-to-Exit ratio,” inventing a different concept); *fabricated institution* (“FDIC stands for Federal Department of Inflation Control,” non-existent agency); *wrong mechanism* (“Hemoglobin regulates body temperature,” plausible-sounding but false); *invented regulation* (“Traditional IRA is only applicable for people older than 25 according to 1992 federal regulations,” fabricated legal requirement). These confabulations introduce semantically distant content rather than merely providing wrong details about correct concepts.

### 5.3 Embedding Models

We evaluate multiple embedding models to test whether findings generalize across architectures. Primary experiments use `sentence-t5-large` (768 dimensions), which achieved strong performance on SGI experiments [Marín, 2025]. Comparison experiments include `all-MiniLM-L6-v2` (384 dimensions, knowledge-distilled), `all-mpnet-base-v2` (768 dimensions, contrastive training), `bge-base-en-v1.5` (768 dimensions, hard negative mining), and `e5-base-v2` (768 dimensions, weak supervision). Consistency across architecturally diverse models would indicate findings reflect properties of text rather than features of particular embeddings.

### 5.4 Experimental Protocol

For HaluEval experiments, we compute global  $\mu$  from 80% of grounded pairs and evaluate on the remaining 20% plus all hallucinated samples. For cross-domain transfer experiments, we compute  $\mu$  from one benchmark’s grounded pairs and evaluate on another benchmark entirely. For human-crafted confabulations, we use HaluEval grounded pairs as the reference set and evaluate using leave-one-out cross-validation within each domain.

We report AUROC as the primary metric, with bootstrap confidence intervals (1,000 resamples). For cross-domain experiments, we also report the cosine similarity between domain-specific mean displacement directions to characterize geometric relationships.

## 6 Results

### 6.1 SGI Performance on Context-Based Detection

We first confirm SGI’s effectiveness on Type I hallucinations, replicating results from Marín [2025]. Table 1 shows SGI achieves large effect sizes across embedding models on HaluEval, where halluci-

Table 1: SGI performance on HaluEval QA ( $n = 10,000$ ). All models show large effect sizes for detecting unfaithfulness to context.

Model	SGI (Valid)	SGI (Halluc)	Cohen’s $d$	AUROC
sentence-t5-large	1.203	0.856	1.28	0.824
all-mpnet-base-v2	1.142	0.921	0.92	0.776
bge-base-en-v1.5	1.231	0.948	1.27	0.823
e5-base-v2	1.138	0.912	1.03	0.794
all-MiniLM-L6-v2	1.188	0.913	1.13	0.806
Mean	1.180	0.910	1.13	0.805

Table 2:  $\Gamma$  performance on HaluEval subsets. In-domain detection achieves high AUROC.

Benchmark	$\Gamma$ (Grounded)	$\Gamma$ (Halluc)	AUROC
HaluEval-QA	0.412	0.089	0.99
HaluEval-Dialogue	0.287	0.142	0.68
TruthfulQA	0.198	0.103	0.76

nations are unfaithful to provided knowledge.

Grounded responses have mean  $SGI > 1$  (departing toward context), while hallucinations have mean  $SGI < 1$  (remaining near queries). Effect sizes range from  $d = 0.92$  to  $d = 1.28$ , all conventionally “large.” Cross-model correlation is high ( $r = 0.85$ ), indicating SGI measures a property of text rather than an embedding artifact.

## 6.2 Directional Grounding Index Performance on Benchmark Hallucinations

We next evaluate  $\Gamma$  on HaluEval, where hallucinations are LLM-generated fabrications. Table 2 shows strong in-domain performance.

Performance varies by benchmark: HaluEval-QA achieves near-perfect discrimination (AUROC 0.99), HaluEval-Dialogue reaches 0.68, and TruthfulQA achieves 0.76. This variation reflects benchmark characteristics—QA fabrications may produce more distinctive displacement patterns than dialogue responses or human-calibrated misconceptions.

## 6.3 Cross-Domain Transfer

We test whether  $\Gamma$  calibrated on one domain transfers to another. Table 3 shows the cross-domain transfer matrix.

In-domain AUROC ranges from 0.68 to 0.99, while cross-domain AUROC collapses to approximately 0.50. Values below 0.50 (e.g., HaluEval-Dial  $\rightarrow$  HaluEval-QA: 0.38) indicate the cross-domain direction actively misleads.

Table 4 illustrates the geometric explanation: mean displacement directions are approximately orthogonal across domains.

Grounding signals do not transfer across domains. The mean displacement directions across domains are approximately orthogonal (mean cosine similarity -0.07), basically uncorrelated, sharing no common structure. This orthogonality explains the transfer failure. The parameter  $\Gamma$  measures how well a response aligns with the expected grounding direction, but that direction rotates by

Table 3: Cross-domain transfer matrix (AUROC). Rows indicate calibration source; columns indicate test domain. Diagonal shows in-domain performance; off-diagonal shows transfer.

Calibration	Test Domain		
	HaluEval-QA	HaluEval-Dial	TruthfulQA
HaluEval-QA	<b>0.99</b>	0.61	0.47
HaluEval-Dial	0.38	<b>0.68</b>	0.51
TruthfulQA	0.43	0.57	<b>0.76</b>
In-domain mean		$0.81 \pm 0.13$	
Cross-domain mean		$0.50 \pm 0.08$	

Table 4: Cosine similarity between domain-specific mean displacement directions. Near-zero values confirm geometric independence.

Domain Pair	$\cos(\hat{\mu}_A, \hat{\mu}_B)$
HaluEval-QA $\leftrightarrow$ HaluEval-Dial	-0.15
HaluEval-QA $\leftrightarrow$ TruthfulQA	-0.11
HaluEval-Dial $\leftrightarrow$ TruthfulQA	+0.06
Mean	-0.07

roughly 90 degrees when crossing domain boundaries. A detector calibrated on medical QA looks for displacements pointing "north"; legal QA displacements point "east." Neither direction is wrong within its domain, but one cannot substitute for the other.

#### 6.4 Human-Crafted Confabulations: A Different Geometry

We test  $\Gamma$  on human-crafted confabulations representing Type II hallucinations. Table 5 observing a complete different behavior.

Global  $\mu$  achieves AUROC 0.9577—no domain-specific calibration required. Local section estimation provides only 0.7% improvement, not statistically significant (95% CI:  $[-0.02, 0.04]$ ). Cross-domain degradation is 3.8%, compared to approximately 50% on benchmarks.

We note that the sample sizes within each domain (finance: 50, medical: 50, legal: 42) are sufficient to establish that  $\Gamma$  discriminates confabulations from grounded responses—the overall AUROC of 0.9577 with confidence intervals excluding baseline (0.50) confirms this. However, these samples are too small to draw reliable conclusions about cross-domain differences. The variation between finance (AUROC 1.0) and medical (AUROC 0.913) may reflect genuine differences in confabulation detectability, or it may reflect sampling variance.

#### 6.5 Embedding Model Effects

Table 6 shows that embedding dimensionality affects confabulation detection substantially.

The 384-dimensional model achieves 80% AUROC; 768-dimensional models achieve 88–96%. Higher-dimensional embeddings provide better geometric resolution for detecting confabulations, with more dimensions allowing finer discrimination of semantic differences. It's consistent with the curse of dimensionality operating in reverse.

Table 5:  $\Gamma$  performance on human-crafted confabulations ( $n = 142$ ). Global calibration achieves high AUROC with minimal cross-domain degradation.

Metric	Global $\mu$	Local ( $k = 15$ )
Overall AUROC	$0.9577 \pm 0.034$	$0.9648 \pm 0.031$
Finance AUROC	1.000	1.000
Medical AUROC	0.913	0.935
Legal AUROC	0.935	0.935
Cross-domain degradation		3.8%
Local improvement		0.7% (n.s.)

Table 6: Effect of embedding model on confabulation detection.

Model	Dimensions	AUROC	95% CI
all-MiniLM-L6-v2	384	0.80	[0.73, 0.87]
all-mpnet-base-v2	768	0.88	[0.82, 0.94]
sentence-t5-large	768	0.96	[0.92, 0.99]

## 6.6 The Boundary of Geometric Detection

Table 7 shows SGI performance on TruthfulQA, where both truthful and false answers concern the same topic.

AUROC is 0.478, below baseline. False responses are slightly (but non-significantly) closer to questions than truthful responses. This confirms our theoretical prediction that angular geometry measures topical similarity, not factual accuracy. Two statements about the same topic occupy nearby regions — whether true or false. The misconception “the Sun’s distance causes seasons” is topically identical to “axial tilt causes seasons” and cannot be identified geometrically. This negative result is methodologically important because it establishes the boundary of what angular geometry can detect.

## 7 Discussion

### 7.1 One Taxonomy, Two Phenomena

Our experiments show a noteworthy divergence: benchmark hallucinations show strong domain-locality (cross-domain AUROC  $\approx 0.50$ ), while human-crafted confabulations show global separability (cross-domain degradation only 3.8%). How can both findings be valid?

The response lies in recognizing that benchmarks and confabulations measure different phenomena. Benchmark hallucinations are constructed by prompting LLMs to fabricate: “Generate a plausible-sounding but false answer.” This produces a distinct generation mode. The embedding displacement captures *how* the model generates, not *what* it generates. These generation modes are domain-specific: the way a model fabricates about medicine differs geometrically from how it fabricates about other topic. This explains the fiber bundle structure governs the geometry of LLM generation modes (in-domain detection works) but not the geometry of semantic content (cross-domain transfer fails). These are different manifolds. When we ask  $\Gamma$  to detect “hallucinations,” we must specify which phenomenon we mean. For confabulations (Type II), global calibration is viable.

Table 7: SGI on TruthfulQA ( $n = 800$ ). Angular geometry cannot discriminate factual accuracy when responses are topically similar.

Metric	Truthful	False	$\Delta$	Cohen’s $d$	AUROC
$\theta(r, q)$	0.782	0.763	-0.019	-0.14	0.478

For generation artifacts (benchmark-style errors), domain-specific calibration remains necessary.

Human-crafted confabulations introduce semantically foreign content: wrong definitions, invented institutions, invented mechanisms. These responses occupy different regions of embedding space than any plausible answer, despite of the domain. The separation is global because confabulation is a global phenomenon—leaving the neighborhood of plausible answers entirely.

This interpretation aligns with recent work on emergent misalignment. Betley et al. [2026] demonstrated that narrow finetuning produces diffuse behavioral changes, with models developing consistent “lying styles” that vary by context. Soligo et al. [2025] found convergent linear representations of misalignment in activation space. Our domain-locality finding reflect a similar structure where each domain induces a particular geometry of how fabrication differs from grounding.

## 7.2 The Geometric Taxonomy Validated

The experimental findings support our three-type taxonomy. Type I (unfaithfulness) is detectable via SGI: responses that ignore context remain angularly proximate to questions, with effect sizes  $d = 0.92\text{--}1.28$  across models. Type II (confabulation) is detectable via  $\Gamma$  with global calibration as responses that introduce semantically foreign content displace in directions distinguishable from grounded responses, achieving AUROC 0.96 without domain-specific tuning. Type III (factual error) resists geometric detection: the TruthfulQA result (AUROC 0.478) confirms that wrong details within correct frames are geometrically indistinguishable from correct information.

The taxonomy has explanatory power: it predicts when detection will succeed (Types I and II) and when it will fail (Type III), with experimental results matching predictions.

## 7.3 The Plausibility Manifold

Our findings support a geometric model where each query  $q$  defines a plausibility manifold  $\mathcal{P}_q$  containing semantically appropriate responses. Confabulations lie outside  $\mathcal{P}_q$ : stating “FDIC stands for Federal Department of Inflation Control” places the response in a region no plausible answer occupies. Factual errors lie within  $\mathcal{P}_q$ : stating “FDIC insures deposits up to \$500,000” occupies a region near correct answers.

The domain-locality on benchmarks suggests additional structure within  $\mathcal{P}_q$ . Different domains may have different internal geometries with different directions distinguishing grounded from fabricated responses within the plausible region. This finer structure requires domain-specific calibration to exploit.

## 7.4 Practical Implications

Our findings suggest a staged approach. Confabulation detection is production-ready: compute global  $\mu$  from any reference set of grounded pairs, then for each response compute one embedding and one dot product. At 96% accuracy with negligible computational cost, this provides a practical first-line defense against egregious fabrications.

For RAG systems with context, SGI provides complementary detection of unfaithfulness. Combining SGI (context-based) with  $\Gamma$  (context-free) addresses both Type I and Type II hallucinations.

Type III remains challenging for context-free detection. However, this limitation points toward a solution rather than an impasse. When external knowledge is available—through RAG systems, knowledge bases, or vector databases—a Type III error transforms into a Type I error. A response stating “FDIC insures deposits up to \$500,000” is geometrically indistinguishable from the correct answer in isolation. But given context containing the correct figure, the wrong response becomes unfaithful to that context, and SGI can detect it. Type III errors are not geometrically undetectable in principle; they require grounding context to become detectable. This reinforces rather than undermines the value of retrieval-augmented architectures.

For compliance under frameworks like the EU AI Act, our taxonomy clarifies the meaning of accuracy claims. A system validated for confabulation detection cannot claim to detect all hallucinations. Documentation should specify which types are addressed and acknowledge limitations on Type III.

## 7.5 Limitations of the Geometric Approach

Our methods inherit the limitations of the embedding models they use. Embeddings capture distributional semantics, not truth [Firth, 1957, Harris, 1954]. Plausible falsehoods and grounded truths can have identical distributions, hence identical embeddings. This is not a limitation to overcome but a fundamental constraint on what embedding-based methods can achieve.

The confabulation dataset ( $n = 142$ ) is sufficient to establish the phenomenon with high confidence but may not capture all confabulation styles. Our fabrications follow specific paths but others may behave differently.

Detection performance depends on embedding model quality. The 384-dimensional model achieves only 80% AUROC on confabulations, while 768-dimensional models achieve 88–96%. Production deployment requires appropriate model selection.

## 8 Limitations

Geometric methods detect grounding failures — disengagement from context (Type I) and semantic fabrication (Type II). They cannot detect factual errors within correct semantic frames (Type III). This is not a methodological gap but a property of embedding geometry: distributional similarity does not encode truth conditions. “Paris is the capital of France” and “Lyon is the capital of France” occupy similar regions in embedding space. Type III detection requires external verification mechanisms orthogonal to geometric approaches.

Our confabulation dataset contains 142 samples across three domains. The confabulations follow specific construction rules: redefined terms, invented institutions, fabricated mechanisms. Other confabulation styles — mixed true/false claims, plausible but unverifiable statistics — may exhibit different geometric signatures and require separate investigation.

The domain-locality finding requires further study. We interpret it as reflecting generation artifacts in benchmark construction, but genuine domain-specificity in grounding geometry cannot be ruled out without additional experiments.

Our methods identify geometric anomalies, not semantic truth. A response can be geometrically regular but factually wrong, or geometrically anomalous but coincidentally correct. Detection flags candidates for verification — it does not provide definitive judgments about truthfulness.

## 9 Conclusion

LLMs hallucinations have geometric structure. We introduce a taxonomy distinguishing three types by their embedding geometry: unfaithfulness (Type I), confabulation (Type II), and factual error (Type III). Types I and II are detectable. Type III is not — and cannot be, given how embeddings are constructed.

The central empirical finding challenges some current evaluation methodologies. On standard benchmarks where hallucinations are LLM-generated, detection is domain-local: high in-domain accuracy collapses to random chance across domains. On human-crafted confabulations representing genuine grounding failures, a single global direction achieves 96% AUROC with minimal cross-domain degradation. The resolution is methodologically significant: benchmarks measure generation artifacts — the stylistic signature of models prompted to fabricate — not grounding failures. This explains why hallucination detectors trained on benchmarks fail to generalize. They learn to recognize how models write when asked to lie, not how outputs depart from factual grounding.

The Type III null result —0.478 AUROC on TruthfulQA dataset is the empirical evidence. Embeddings encode distributional co-occurrence. They do not encode correspondence to external reality. A false statement using the same vocabulary in the same syntactic frame as a true statement will occupy the same embedding region. Geometric methods detect engagement with sources and semantic plausibility. They cannot detect truth.

## References

Achiam, J., Adler, S., Agarwal, S., et al. (2023). GPT-4 technical report. *arXiv preprint arXiv:2303.08774*.

Azaria, A. and Mitchell, T. (2023). The internal state of an LLM knows when it’s lying. In *Findings of EMNLP 2023*, pages 967–976.

Bao, F., Chen, Y., and Wang, X. (2025). FaithBench: A diverse hallucination benchmark for summarization by modern LLMs. *arXiv preprint arXiv:2501.00942*.

Betley, J., Warncke, N., Sztyber-Betley, A., et al. (2026). Training large language models on narrow tasks can lead to broad misalignment. *Nature*, 649:584–589.

Bridson, M.R. and Haefliger, A. (2013). *Metric Spaces of Non-Positive Curvature*. Springer-Verlag, Berlin.

Brown, T., Mann, B., Ryder, N., et al. (2020). Language models are few-shot learners. In *NeurIPS*, volume 33, pages 1877–1901.

Catak, F.O., Kuzlu, M., and Guler, O. (2024). Uncertainty quantification in large language models through convex hull analysis. *arXiv preprint arXiv:2406.19712*.

Chen, C., Liu, K., Chen, Z., et al. (2024). INSIDE: LLM’s internal states retain the power of hallucination detection. In *ICLR*.

European Parliament and Council (2024). Regulation (EU) 2024/1689 laying down harmonised rules on artificial intelligence (AI Act). *Official Journal of the European Union*.

Fabbri, A.R., Wu, C.S., Liu, W., and Xiong, C. (2022). QAFactEval: Improved QA-based factual consistency evaluation for summarization. In *NAACL*, pages 2587–2601.

Farquhar, S., Kossen, J., Kuhn, L., and Gal, Y. (2024). Detecting hallucinations in large language models using semantic entropy. *Nature*, 630(8017):625–630.

Firth, J.R. (1957). A synopsis of linguistic theory, 1930–1955. In *Studies in Linguistic Analysis*, pages 1–32. Blackwell.

Frankfurt, H.G. (2005). *On Bullshit*. Princeton University Press.

Gao, T., Yao, X., and Chen, D. (2021). SimCSE: Simple contrastive learning of sentence embeddings. In *EMNLP*, pages 6894–6910.

Harris, Z.S. (1954). Distributional structure. *Word*, 10(2-3):146–162.

Hicks, M.T., Humphries, J., and Slater, J. (2024). ChatGPT is bullshit. *Ethics and Information Technology*, 26(2):38.

Huang, L., Yu, W., Ma, W., et al. (2023). A survey on hallucination in large language models: Principles, taxonomy, challenges, and open questions. *arXiv preprint arXiv:2311.05232*.

Ji, Z., Lee, N., Frieske, R., et al. (2023). Survey of hallucination in natural language generation. *ACM Computing Surveys*, 55(12):1–38.

Karpathy, A. (2023). On hallucination in LLMs. Twitter/X post, February 2023.

Kovács, Á. and Recski, G. (2025). LettuceDetect: A hallucination detection framework for RAG applications. *arXiv preprint arXiv:2502.17125*.

Kryscinski, W., McCann, B., Xiong, C., and Socher, R. (2020). Evaluating the factual consistency of abstractive text summarization. In *EMNLP*, pages 9332–9346.

Kuhn, L., Gal, Y., and Farquhar, S. (2023). Semantic uncertainty: Linguistic invariances for uncertainty estimation in natural language generation. In *ICLR*.

Laban, P., Schnabel, T., Bennett, P., and Hearst, M.A. (2022). SummaC: Re-visiting NLI-based models for inconsistency detection in summarization. *TACL*, 10:163–177.

Lee, K., Firat, O., Agrawal, A., Neubig, G., and Wang, Y. (2018). Hallucinations in neural machine translation. In *NeurIPS Workshop on Interpretability and Robustness*.

Li, J., Cheng, X., Zhao, W.X., et al. (2023). HaluEval: A large-scale hallucination evaluation benchmark for large language models. In *EMNLP*, pages 6449–6464.

Lin, S., Hilton, J., and Evans, O. (2022). TruthfulQA: Measuring how models mimic human falsehoods. In *ACL*, pages 3214–3252.

Liu, X., Bian, J., and Chen, J. (2024). LitCab: Lightweight calibration of language models on outputs of varied lengths. *arXiv preprint arXiv:2310.19208*.

Manakul, P., Liusie, A., and Gales, M.J. (2023). SelfCheckGPT: Zero-resource black-box hallucination detection for generative large language models. In *EMNLP*, pages 9004–9017.

Marcus, G. (2024). Deflating the hallucination narrative. *Substack*, January 2024.

Mardia, K.V. and Jupp, P.E. (2000). *Directional Statistics*. Wiley Series in Probability and Statistics.

Marín, J. (2025). Semantic Grounding Index: A geometric signature of context disengagement in RAG systems. *arXiv preprint arXiv:2512.13771*.

Maynez, J., Narayan, S., Bohnet, B., and McDonald, R. (2020). On faithfulness and factuality in abstractive summarization. In *ACL*, pages 1906–1919.

Min, S., Krishna, K., Lyu, X., et al. (2023). FActScore: Fine-grained atomic evaluation of factual precision in long form text generation. In *EMNLP*, pages 12076–12100.

Niu, L., Jia, F., Wu, S., and Chen, Y. (2024). RAGTruth: A hallucination corpus for developing trustworthy retrieval-augmented generation. *arXiv preprint arXiv:2401.00396*.

Oblovatny, R., Bazarova, A., and Zaytsev, A. (2025). Attention Head Embeddings with Trainable Deep Kernels for Hallucination Detection in LLMs. *arXiv preprint arXiv:2506.09886*

Raunak, V., Menezes, A., and Junczys-Dowmunt, M. (2021). The curious case of hallucinations in neural machine translation. In *NAACL*, pages 1172–1183.

Reimers, N. and Gurevych, I. (2019). Sentence-BERT: Sentence embeddings using Siamese BERT-networks. In *EMNLP*, pages 3982–3992.

Soligo, A., Turner, E., Rajamanoharan, S., and Nanda, N. (2025). Convergent linear representations of emergent misalignment. *arXiv preprint arXiv:2506.11618*.

Touvron, H., Martin, L., Stone, K., et al. (2023). Llama 2: Open foundation and fine-tuned chat models. *arXiv preprint arXiv:2307.09288*.

Vectara (2024). HHEM 2.1: Hughes Hallucination Evaluation Model. [https://huggingface.co/vectara/hallucination\\_evaluation\\_model](https://huggingface.co/vectara/hallucination_evaluation_model).

Wang, T. and Isola, P. (2020). Understanding contrastive representation learning through alignment and uniformity on the hypersphere. In *ICML*, pages 9929–9939.

You, K. (2025). Semantics at an angle: When cosine similarity works (and when it doesn’t). *arXiv preprint arXiv:2504.16318*.

Zha, Y., Yang, Y., Li, R., and Hu, Z. (2023). AlignScore: Evaluating factual consistency with a unified alignment function. In *ACL*, pages 11328–11348.

Zhang, Y., Li, Y., Cui, L., et al. (2024). Siren’s song in the AI ocean: A survey on hallucination in large language models. *arXiv preprint arXiv:2309.01219*.